Available online at www.sciencedirect.com

SCIENCE DIRECT®

Earth and Planetary Science Letters 225 (2004) 243–251

EPSL

www.elsevier.com/locate/epsl

Elastic anisotropy in textured hcp-iron to 112 GPa from sound wave propagation measurements

Daniele Antonangeli[a,*], Florent Occelli[a], Herwig Requardt[a], James Badro[b], Guillaume Fiquet[b], Michael Krisch[a]

[a] *European Synchrotron Radiation Facility, BP 220, 38043 Grenoble, France*
[b] *Laboratoire de Minéralogie-Cristallographie de Paris, UMR CNRS 7590, Université Paris VI, Institut de Physique du Globe de Paris, 4 Place Jussieu, 75252 Paris, France*

Received 3 December 2003; received in revised form 30 April 2004; accepted 7 June 2004

Editor: V. Courtillot

Abstract

We report the first experimental determination of elastic anisotropy in highly textured polycrystalline hexagonal-closed-packed (hcp)-iron obtained at room temperature and 112 GPa by inelastic X-ray scattering (IXS) in a diamond anvil cell (DAC). The compressional sound velocity V_P at 50° and 90° from the *c*-axis was determined to be $V_P\{50°\} = 9900 \pm 200$ m/s and $V_P\{90°\} = 9450 \pm 150$ m/s, respectively. The difference of 4–5% between the two velocities is of the same order of the seismic observations of the anisotropy in Earth's inner core. Combining our new results with the equation of state of hcp-iron, we derive the pressure dependence of the shear velocity V_S. The V_S-values, extrapolated to inner core densities, are 30% higher than the PREM results. The extrapolated V_P-values are instead in fair agreement with the PREM seismic model, though differences in the slope remain. Furthermore, assuming a strong texture characterized by cylindrical symmetry, we provide an estimate for the single crystal elastic modulus C_{11} as a function of pressure. While our results are in general agreement with the predominant existence of hcp-iron in Earth's inner core, the remaining differences might be assigned to the presence of another solid iron phase, light elements, or liquid inclusions as well as anharmonic high-temperature effects.

Keywords: hcp-iron; elastic anisotropy; Earth's inner core; sound velocities; inelastic x-ray scattering; high pressure

1. Introduction

Present theories consider the Earth's inner core to be predominantly composed of solid iron, alloyed with some light element(s) in order to account for a 4% to 5% deficit in density with respect to pure hexagonal-closed-packed (hcp)-iron [1,2]. Amongst the possible high-pressure crystallographic structures of iron, the hcp or ε-phase is the one generally considered most relevant for Earth's core, since it is stable to at least 300 GPa at ambient temperature [3], although other structures, such has dhcp [4,5], bcc [6], or orthorhom-

* Corresponding author. Tel.: +33-4-76-88-23-92; fax: +33-4-76-88-29-04.
E-mail address: antonangeli@esrf.fr (D. Antonangeli).

0012-821X/$ - see front matter © 2004 Elsevier B.V. All rights reserved.
doi:10.1016/j.epsl.2004.06.004

bic [7] phases have been proposed as well. It is by now well established that the Earth's inner core is elastically anisotropic [8–12], with seismic waves travelling along the rotation axis 3–4% faster than those propagating in the equatorial plane. Current experimental and theoretical efforts aim to identify the underlying mechanisms responsible for such anisotropy. In general, alignment of iron crystals is required to explain this feature, but proposed mechanisms for generating the texture differ in the dynamical forcing (i) by the magnetic field of the outer core as it solidifies at the inner core boundary [13], (ii) by large-scale convective flow in the inner core [14,15] or (iii) by the remains of preferential orientation from the growth of the crystals [16], and (iv) by the development of anisotropy as the inner core deforms plastically under the influence of electromagnetic shear stresses [17]. Differentiation between the various models is to a great degree hampered by the dearth of experimental data at relevant pressures and temperatures. Prior to the present study, the only experimental results on elastic anisotropy were obtained using X-ray radial diffraction (XRD) on textured ε-iron to 211 GPa at room temperature [18], but the assumptions necessary for the analysis limit the reliability of the results [19]. The variation of the longitudinal (compressional) sound velocity V_P in the meridian plane proposed in [18] is shown in Fig. 1 along with theoretical results. At both pressures investigated in this experiment (39 and 211 GPa), the curve has a "bell-like" shape with a maximum sound anisotropy—defined as $2 \times (V_{max} - V_{min})/V_{max} + V_{min})$—of about 8% at 45° from the basal plane (a), and almost identical sound velocities along the a- and c-axes. Theoretical results show differences not only in magnitude [20], but as well in shape [21–25], and furthermore emphasise the importance of temperature on the elastic properties [24,25]. Possible causes for these discrepancies are (i) the difficulty to perform reliable calculations at core conditions as evidenced for example in [26], and (ii) the impossibility to carry out experiments on single crystal hcp-iron due to the bcc-to-hcp transition around 13 GPa. The discrepancies amongst the various calculations, and these studies and experimental results, clearly demonstrate the need to perform further experimental work and have motivated the present study.

Here we report the first direct experimental determination of the anisotropy in the propagation

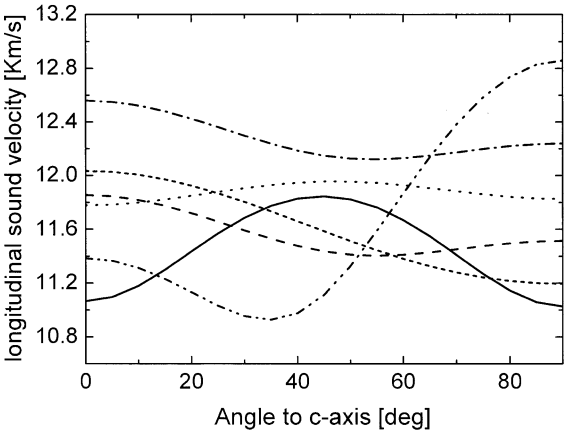

Fig. 1. Longitudinal sound velocity V_P as a function of propagation direction in the meridian (a–c plane) for hcp-iron at 211 GPa. XRD measurements [18]: solid line. Calculations at 0 K: dashed line [21,23]; dotted line [20]; dash-dotted line [22]. Short dashed line: calculations at 210 GPa and 300 K [24]. Dash-dot-dotted line: calculation at 6000 K for a density of 13 mg/m^3 [25].

of longitudinal acoustic waves in iron at high pressure by inelastic X-ray scattering (IXS). In an ideal, randomly oriented powder, IXS probes the orientationally averaged longitudinal sound dispersion. On the other hand, it is well known that hcp-iron develops strong lattice preferred orientations when uniaxially compressed in a diamond anvil cell (DAC). This preferred orientation, or texture, has been determined by X-ray diffraction [18,27,28], showing that, with increasing pressure, the c-axis preferentially aligns along the main compression axis of the cell. Utilising different scattering geometries relative to the DAC compression axis, it is possible to determine V_P for different propagation directions, intermediate between the c-axis and the basal plane. We also present a new analysis of the pressure evolution of the compressional velocity V_P as well as results for the shear velocity V_S and the elastic modulus C_{11}. Our IXS results are compared with other experimental and theoretical data, and implications for the sound wave propagation in Earth's inner core are discussed.

2. Experimental set-up

Our IXS experiments were performed on beamline ID28 at the European Synchrotron Radiation

Facility (ESRF) in Grenoble, France [29]. We used the Si (8 8 8) configuration, yielding a total instrumental energy resolution of 5.6 meV full-width-half-maximum (FWHM). The transverse dimensions of the focused X-ray beam were 0.25 horizontal × 0.06 vertical mm^2 (FWHM). These incident beam dimensions were further reduced by slits in order to avoid scattering from the pressure cell gasket. The scattered photons were energy-analysed by five crystals in Rowland circle geometry working at the same reflection order as the high-resolution backscattering monochromator. The momentum transfer, $Q=2k_0\sin(\theta_s/2)$, where k_0 is the wave vector of the incident photons and θ_s the scattering angle, was selected by rotating the spectrometer arm in the horizontal plane. The Q resolution was set by slits in front of the analysers to 0.2 nm^{-1}.

Polycrystalline 99.99% iron from Sigma Aldrich was loaded in a 90 μm diameter hole drilled in a rhenium gasket, pre-indented to a thickness of 28 μm (initially 200 μm), and pressurized in a diamond anvil cell equipped with bevelled diamonds (150 μm flat bevelled from 300 μm culets at an angle of 8°). No pressure-transmitting medium was used. The cell was specifically designed with a rectangular slit opening of 96 × 10° (parallel and perpendicular to the scattering plane, respectively). Thus two different geometries were employed (see Fig. 2), corresponding to a longitudinal sound propagation of 50° and 90° with respect to the loading axis. Pressure was determined in situ by the ruby fluorescence technique and crosschecked by X-ray diffraction using the equation of state of iron [3].

3. Results

3.1. Experimental data and analysis

The data were collected at room temperature and at two different pressures (22 and 112 GPa), recording up to nine Q-values (between 4 and 13 nm^{-1}) for the two orientations. Fig. 3 shows typical IXS spectra for two momentum transfers and orientations of the DAC at 112 GPa. The spectra are characterized by an elastic contribution, centred at zero energy, and inelastic contributions from iron and diamond. The transverse acoustic (TA) phonons of diamond are located at higher energies with respect to iron because of their higher sound velocity, and appear as rising slopes at the high energy end of the investigated spectral range. The longitu-

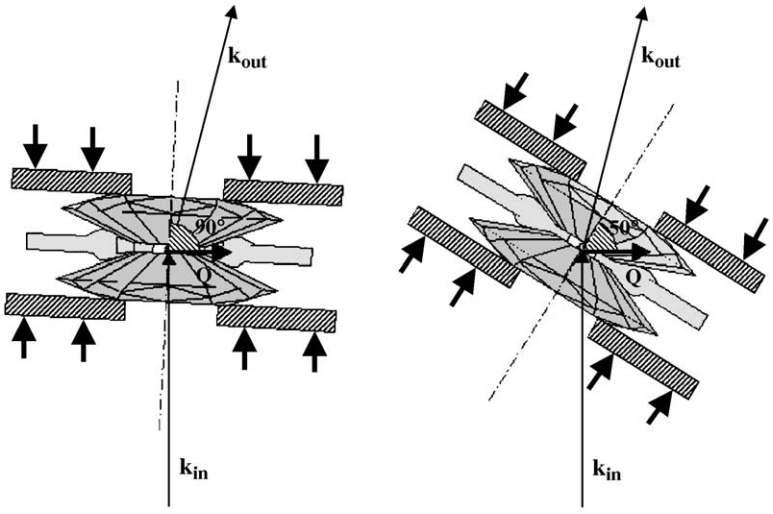

Fig. 2. Schematic representation of the diamond anvil cell and the two different scattering geometries: k_{in} and k_{out} denote the incident and scattered photon wave-vector, respectively. The dash-dotted line indicates the load axis of the DAC. The propagation direction of the probed sound waves, given by Q, and their angle with respect to the load axis are indicated as well.

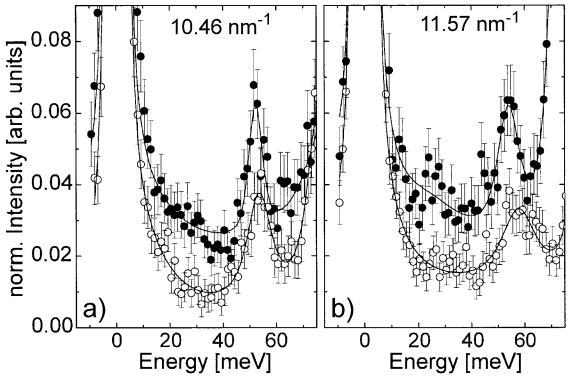

Fig. 3. IXS spectra of hcp-iron at room temperature and 112 GPa for two different orientations of the DAC: full (open) circles: sound propagation at 90° (50°) to the DAC loading axis. The experimental data and their statistical error bars are shown together with their best fits. The momentum transfer values, at which the spectra were recorded, are indicated in the figures. The low count rate required an integration time around 1000 s per point, resulting in a total acquisition time of 2 days per dispersion curve.

dinal acoustic (LA) phonon of iron is therefore unambiguously identified as peak between the diamond phonon and the elastic line. In each scan the full elastic line has been recorded. This allowed a robust determination of the zero energy position. The energy position of the iron phonons were extracted by fitting a set of Lorentzian functions convoluted with the experimental resolution function to the IXS spectra, utilizing a standard χ^2 minimisation routine. For both momentum transfers shown in Fig. 3, the iron phonon in the "50°-configuration" is observed at higher energies than in the "90°-configuration"; this is especially true for $Q = 11.57$ nm^{-1} where the energy difference amounts to several meV. This observation is further validated by the inspection of the complete dispersion curves, which are reported in Fig. 4. At 22 GPa the phonon energies are essentially the same for the two orientations of the cell, whereas the two dispersions at 112 GPa clearly show that, for each given momentum transfer, higher phonon energies are observed in the case of the "50°-configuration", suggesting that there is a considerable sound propagation anisotropy. Due to the low contrast of the iron phonon peak with respect to the elastic line at low Q, IXS data could not be recorded in the linear part of the dispersion, where the sound velocity is proportional to the slope of the curve. As a consequence, reasonable assumptions concerning the shape of the dispersion curve have to be made, in order to extract the value of the sound velocity.

Within the framework of the Born–von Karman lattice-dynamics theory, the solution of the dynamical matrix can be written as [30]:

$$M\omega^2 = \sum_n \Phi_n \left[1 - \cos\left(n\pi \frac{Q}{Q_{\max}}\right)\right] \quad (1)$$

where M is the atomic mass, ω the angular frequency and Q the wave vector of the considered normal mode, $Q_{\max}$ is half the distance to the nearest reciprocal lattice point in the direction of Q, and Φ_n the interplanar force constants (the force between an atom and the nth neighbour plane normal to Q). Limiting us to the first term in the expansion (nearest neighbour interaction), and con-

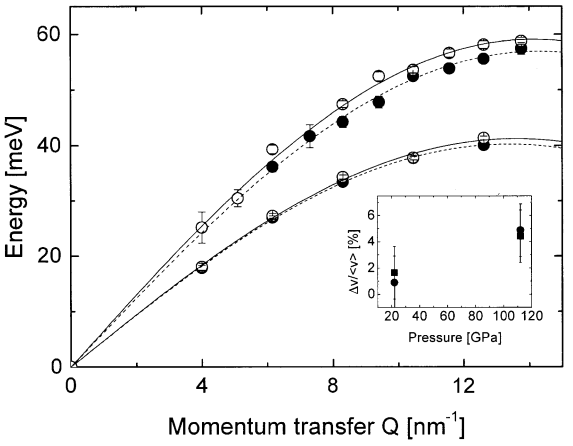

Fig. 4. LA phonon dispersion curves of iron at room temperature and at pressures P of 22 GPa (lower curve) and 112 GPa (upper curve) for the two orientations of the DAC; full (open) circles: sound propagation at 90° (50°) to the DAC loading axis. The displayed error bars of the energy position results from the statistic error of the fit and the finite Q-resolution of the spectrometer. The lines through the data points are fits to the data, with $Q_{\max}$ as a free parameter. The inset reports the relative difference of the sound speeds $\Delta v/\langle v\rangle$ as a function of pressure. The two methods used to derive the sound speed (see Section 3.1) yield slightly different results, indicated by full circles ($Q_{\max}$ free) and squares ($Q_{\max}$ fixed).

verting the equation into a form suitable to fit the experimental data, one obtains:

$$E[\mathrm{meV}] = 2.964 \times 10^{-4} V_P[\mathrm{m/s}] \times Q_{\max}[\mathrm{nm}^{-1}] \times \sqrt{1 - \cos\left(\frac{\pi Q[\mathrm{nm}^{-1}]}{Q_{\max}[\mathrm{nm}^{-1}]}\right)} \quad (2a)$$

or equivalently

$$E[\mathrm{meV}] = 4.192 \times 10^{-4} V_P[\mathrm{m/s}] \times Q_{\max}[\mathrm{nm}^{-1}] \sin\left(\frac{\pi}{2} \frac{Q[\mathrm{nm}^{-1}]}{Q_{\max}[\mathrm{nm}^{-1}]}\right) \quad (2b)$$

Inspection of Eqs. (2a) and (2b) shows that the resulting value of the sound velocity critically depends on the value of $Q_{\max}$. Its value can be unambiguously determined in single crystals, while a correct averaging scheme including the effect of texture has to be employed in the case of polycrystalline samples. In the present case, $Q_{\max}$ was determined in two different ways: (i) a set of 10,000 vectors with their origin at the Γ point and random orientation were generated and their intersection with the Wigner–Seitz Brillouin zone (BZ) boundary was determined. $Q_{\max}$ was then derived from the average length of these 10,000 vectors. (ii) $Q_{\max}$ is left a free parameter in the fit. The first method has the advantage to reduce the correlation between the parameters and to ensure the reliability of the $Q_{\max}$-value, but it does not include the effect of preferred orientation, while the second naturally takes it into account. The $Q_{\max}$ values given by the two methods differ by about 2% to 3%, while the differences in sound speed are typically less then 2%. The accuracy on the determination of sound velocities, considering the statistical error of the fits, the error on pressure determination as well as a possible pressure gradient up to ± 10 GPa at the highest pressure, and the correlation with the values of $Q_{\max}$, is between 2% and 3%.

3.2. Sound wave anisotropy

Fig. 4 shows the best fits to the dispersion curves at room temperature for the two orientations of the DAC at pressures of 22 and 112 GPa with $Q_{\max}$ left as a free parameter. The inset reports the sound velocity differences. At 22 GPa, the sound velocities differ by 0.9%. This difference increases to 1.6% if $Q_{\max}$ is fixed according to the procedure described earlier. In both cases, however, these differences are within the error bars (2%), and the sound velocities for the two orientations can be considered to be identical. At 112 GPa, the difference in the dispersion curves becomes significant. When keeping $Q_{\max}$ free, the fitted values yield $Q_{\max}\{50°\} < Q_{\max}\{90°\}$, in qualitative agreement with the known preferred orientation of the c-axis along the loading axis. The sound velocities then differ by about 4.8%. When using the procedure to fix $Q_{\max}$, and keeping in mind that it is less justified due to the well-developed texture at such pressures, the difference is reduced to 4.4%. Most importantly, in both cases the difference is significant and outside the error bars. It can therefore be firmly concluded that the sound propagates faster by 4% to 5% at 50° from the c-axis than at 90° (i.e. in the basal plane), with $V_P\{50°\} = 9900 \pm 200$ m/s and $V_P\{90°\} = 9450 \pm 150$ m/s (average of the values determined by the two procedures).

The measured anisotropy on a textured polycrystalline sample at 112 GPa is comparable to that observed in Earth's inner core (3% to 4%) [8–12]. This result directly negates the first-principle calculation [21] that suggested that a nearly perfectly oriented single crystal was needed in order to account for the geophysical observations. Conversely, the texture generated in a DAC without pressure transmitting medium with a dominating c-axis fibre component [28] aligned parallel to the loading axis of the DAC is sufficient to explain Earth's core elastic anisotropy. This conclusion is even more robust in the sense that, while our experiments have been performed at pressures significantly lower than that of Earth's inner core, we find a positive correlation between anisotropy and pressure. Furthermore, recent calculations performed at core temperatures [25] suggest that the amplitude of the anisotropy is increased by a factor two when compared to 0 K results (see Fig. 1). According to these results, even less preferred orientation of hcp-iron crystals could account for the observed seismic anisotropy.

3.3. Pressure evolution of V_P and V_S

These new IXS data allow us to extend previous IXS results [31]. In particular, it has been possible to record the dispersion at 112 GPa with better statistics and more Q points than previously [31], which in turn allows a more robust extrapolation to higher pressures. Fig. 5 reports the density evolution of V_P, for which the whole data set was analysed utilising the procedure described in Section 3.1, together with the results obtained by other experimental techniques and calculations. We use the density–velocity representation to display the data. Within the quasi-harmonic approximation, this allows to compare results that were obtained at different pressure or temperature conditions, and V_P is expected to scale linearly with density (Birch law [32]). The IXS values for V_P compare well with the ultrasonic measurements reported in [18] at low pressure, and follow a nearly linear evolution with density with a larger slope than previously reported. A linear extrapolation to higher densities is closer to the V_P values given by the PREM seismic model [33]. As a matter of fact, the linear extrapolations of the two sets of IXS data (Q_{max} free and fixed) straddle the seismic data [33].

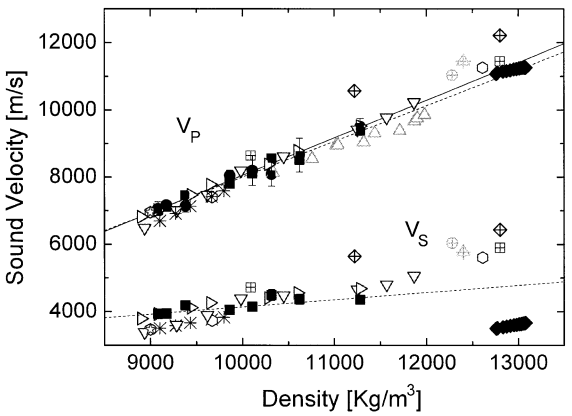

Fig. 5. Aggregate compressional (V_P) and shear (V_S) velocities as a function of density. No texture and temperature effects have been considered. Solid circles (squares): IXS results with the parameter Q_{max} left free (Q_{max} fixed); the lines represent linear fits to the density evolution of the IXS data: solid line (Q_{max} free), dashed line (Q_{max} fixed). Measurements: side-triangles, ISLS results [34]; upside-down triangles, NRIXS data [35]; hexagons and asterisks, XRD data [18,36]; triangles, shock wave Hugoniot measurements [37]; star, ultrasonic measurements [18]. Calculations: crossed squares [21,23]; crossed circles [20]; crossed diamonds [22]; crossed triangles [24]. Preliminary Reference Earth Model seismic data [33] are reported for comparison as full diamonds.

Our measurements are in good agreement with recent results obtained by impulsive stimulated light scattering (ISLS) [34]. We furthermore note a substantial agreement with NRIXS [35] and XRD [18] measurements in a density range between 9500 and 12,000 kg/m^3, partly reconciling the discrepancies observed between IXS results of [31] and NRIXS measurements [35]. At lower densities, a disagreement still persists, even in comparison with other XRD measurements [36]. The longitudinal sound velocities derived from shock wave measurements [37] are lower by 3–4% than all other experimental data determined at room temperature, indicating that anharmonic effects gain an increasing importance at high temperature [18,24]. In contrast, velocities determined through theoretical calculations [20–24] are systematically higher than experimental data.

Combining our results for V_P with the measured density ρ and the bulk modulus K obtained from the ε-iron equation of state, one can derive the shear velocity V_S [38] according to:

$$V_S^2 = \frac{3}{4}\left(V_P^2 - \frac{K}{\rho}\right) \quad (3)$$

In the present case we utilised the equation of state derived from XRD measurements carried out under analogue (i.e. non-hydrostatic) conditions [18,36]. The resulting density evolution of V_S is reported in the lower part of Fig. 5. For clarity, only the IXS data set for which V_P was determined keeping Q_{max} fixed is reported (employing the other method gives results that differ by a few percent). In the case of V_S as well, we observe substantial agreement with the ISLS results [34]. In the density region between 9000 and 10,000 kg/m^3 the IXS data lie slightly above the NRIXS [35] and XRD [18,36] results. This is a direct consequence of the higher V_P values in this density region. The overall agreement is, however, still satisfactory, although a linear fit to the IXS data shows a reduced slope as a function of density with respect the trend of NRIXS and XRD. We note that, independently of the particular experimental data set

used, an extrapolation to core densities leads to V_S values that are significantly higher than what is shown by the PREM model. This observation is in agreement with theoretical results [24], which showed that the shear modulus for ε-iron at core pressures is reduced by 70% going from room temperature to 5400 K. It has also been speculated that partial melting could occur in the inner core, dramatically reducing the composite shear velocities (with respect to pure crystalline hcp-iron) in that region [39] measured by seismic inversion models such as PREM.

3.4. Estimation of C_{11}

XRD measurements [18,27,28] and simulations [28] suggest that the texture of ε-iron in a DAC displays a cylindrical symmetry with a predominant alignment of the *c*-axis parallel to the compression axis of the high-pressure cell. Under these specific conditions, the expression for the compressional wave velocity reduces to [40]:

$$\rho V_P^2\{\xi\} = C_{11} + (4C_{44} + 2C_{13} - 2C_{11})\cos^2(\xi) + (C_{33} + C_{11} - 4C_{44} - 2C_{13})\cos^4(\xi) \quad (4)$$

where ξ is the angle between the direction of propagation and the loading axis of the cell, and C_{ij} are the elastic moduli. For sound propagation at 90° the upper relation reduces to:

$$\rho V_P^2\{90°\} = C_{11} \quad (5)$$

From the IXS data we can therefore estimate the elastic modulus C_{11}. The results are reported as a function of pressure in Fig. 6, together with the values derived from XRD measurements [18,27] and calculations [20–24]. We note a good agreement between the IXS and XRD results and theoretical results by Laio et al. [24], while other calculations [20–23] tend to over-estimate C_{11}. One possible reason could be the fact that the work by Laio et al. is the only one performed at the same temperature as the experiments (300 K), while the others are performed at 0 K, although calculations by Steinle-Neumann et al. [25] predict an increase of C_{11} with temperature. However, the reliability of such calculations at high temperature is strongly dependent on the chosen approximations, and these results are consequently still debated [26].

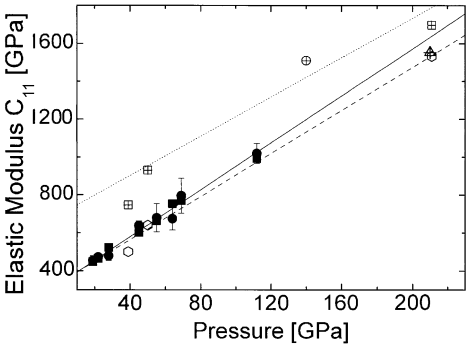

Fig. 6. Derived elastic modulus C_{11} as a function of pressure. Full circles (squares): IXS data analysed with Q_{max} free (fix), solid (dashed) line: corresponding linear fits to the IXS data with Q_{max} free (fix); hexagons: XRD data [18,27]. All the experimental results are at room temperature. Calculations at 0 K: crossed squares [21,23], crossed circles [20], and dotted line [22]. Calculations at 300 K: crossed triangles [24].

4. Conclusions

The main result of the present study is the evidence for a measurable anisotropy in sound wave propagation in hcp-iron, which constitutes a new step towards the characterisation of the elastic properties of iron in Earth's core conditions. The current set of IXS data is limited to two propagation directions, namely 90° and 50° with respect to the *c*-axis, which does not allow us to distinguish between the various schemes of anisotropy of longitudinal acoustic wave propagation as presented in Fig. 1. It has to be stressed, however, that the observed sound velocity difference of 4% at 112 GPa is already of the same order of the anisotropy shown by seismic observations in the Earth's inner core, suggesting that only a moderate alignment of hcp-iron is sufficient to explain such elastic anisotropy. In this context, the effect of temperature on the elastic moduli is potentially important and should be carefully considered [25,26]. Further information can be gained by spanning the full range of propagation

direction between the *a*- and *c*-axes thus putting important constraints on the shape of the sound velocity anisotropy, and consequently on the values of the elastic moduli C_{ij}.

The density evolution of V_P, extrapolated to core pressures, is in reasonable agreement with the PREM, though we note that there is a visible difference in the slope. Possible reasons for this are the presence of other elements in the core, as well as high-temperature anharmonic effects. An indication of this temperature effect is provided by the comparison of the whole set of data collected by different techniques at room temperature with the shock wave results [37], which yield systematically lower values for V_P. The effect of temperature and/or light elements on the shear velocity V_S is much more significant, where both experimental and theoretical results at 0 K or room temperature lie well above the PREM data. Experiments that could probe the effect of temperature or light elements should provide important insights for iron shear properties at core conditions.

Acknowledgements

We wish to thank Daniel Farber for feedback and suggestions with the manuscript. Keith Martel and Denis Gambetti are acknowledged for the design of the DAC sample chamber and help in the experimental setup. Alessandro Mirone is acknowledged for his help with Montecarlo calculations.

References

[1] F. Birch, Elasticity and constitution of the Earth's interior, J. Geophys. Res. 57 (1952) 227–286.
[2] A. Jephcoat, P. Olson, Is the inner core of the Earth pure iron? Nature 325 (1987) 332–335.
[3] H.K. Mao, Y. Wu, L.C. Chen, J. Shu, A.P. Jephcoat, Static compression of iron to 300 GPa and $Fe_{0.8}$ $Ni_{0.2}$ alloy to 260 GPa: implications for composition of the core, J. Geophys. Res. 95 (1990) 21737–21742.
[4] S.K. Saxena, G. Shen, P. Lazor, Experimental evidence for a new iron phase and implications of Earth's core, Science 260 (1993) 1312–1314.
[5] S.K. Saxena, L.S. Dubrovinsky, P. Haggkvist, Y. Cerenius, G. Shen, H.K. Mao, Synchrotron X-ray study of iron at high pressure and temperature, Science 269 (1995) 1703–1704.
[6] A.B. Belonoshko, R. Ahuja, B. Johansson, Stability of the body-centred-cubic phase of iron in the Earth's inner core, Nature 424 (2003) 1032–1034.
[7] D. Andrault, G. Fiquet, M. Kunz, F. Visocekas, D. Haüsermann, The orthorhombic structure of iron: an in situ study at high-temperature and high-pressure, Science 278 (1997) 831–834.
[8] J.H. Woodhouse, D. Giardini, X.D. Li, Evidence for inner core anisotropy from free oscillations, Geophys. Res. Lett. 13 (1986) 1549–1552.
[9] J. Tromp, Support for anisotropy of the Earth's inner core from free oscillations, Nature 366 (1993) 678–681.
[10] B. Romanowicz, X.D. Li, J. Durek, Anisotropy in the inner core: could it be due to low-order convection? Science 274 (1996) 963–966.
[11] X. Song, Anisotropy of the Earth's inner core, Rev. Geophys. 35 (1997) 297–313.
[12] R. Garcia, A. Souriau, Inner core anisotropy and heterogeneity level, Geophys. Res. Lett. 27 (2000) 3121–3124 (correction Geophys. Res. Lett. 28 (2000) 85–86).
[13] S. Karato, Inner core anisotropy due to magnetic field-induced preferred orientation of iron, Science 262 (1993) 1708–1711.
[14] R. Jeanloz, H.R. Wenk, Convection and anisotropy of the inner core, Geophys. Res. Lett. 15 (1988) 72–75.
[15] S. Yoshida, I. Sumita, M. Kumazawa, Growth model of the inner core coupled with the outer core dynamics and the resulting elastic anisotropy, J. Geophys. Res. 101 (1996) 28085–28104.
[16] M.I. Bergman, Measurements of elastic anisotropy due to solidification texturing and the implications for the Earth's inner core, Nature 389 (1997) 60–63.
[17] B.A. Buffet, H.R. Wenk, Texturing of the inner core by Maxwell stresses, Nature 413 (2001) 60–64.
[18] H.K. Mao, J. Shu, G. Shen, R.J. Hemley, B. Li, A.K. Singh, Elasticity and rheology of iron above 220 GPa and the nature of the Earth's inner core, Nature 396 (1998) 741–743 (correction, Nature 399 (1999) 280).
[19] S. Matthies, S. Merkel, H.R. Wenk, R.J. Hemley, H.K. Mao, Effects of texture on the determination of elasticity of polycrystalline ε-iron from diffraction measurements, Earth Planet. Sci. Lett. 194 (2001) 201–212.
[20] P. Söderlind, J.A. Moriarty, J.M. Wills, First principles theory of iron up to Earth-core pressure: structural, vibrational, and elastic properties, Phys. Rev., B 53 (1996) 14063–14072.
[21] L. Stixrude, R.E. Cohen, High-pressure elasticity of iron and anisotropy of Earth's inner core, Science 267 (1995) 1972–1975.
[22] R.E. Cohen, L. Stixrude, E. Wasserman, Tight-binding computations of elastic anisotropy of Fe, Xe, and Si under compression, Phys. Rev., B 56 (1997) 8575–8589 (errata, Phys. Rev. B 58 (1997) 5873).
[23] G. Steinle-Neumann, L. Stixrude, R.E. Cohen, First-principles elastic constants for hcp transition metals Fe, Co, and Re at high pressure, Phys. Rev., B 60 (1999) 791–799.
[24] A. Laio, S. Bernard, G.L. Chiarotti, S. Scandolo, E. Tosatti, Physics of iron at Earth's core conditions, Science 287 (2000) 1027–1030.
[25] G. Steinle-Neumann, L. Stixrude, R.E. Cohen, O. Gülseren,

Elasticity of iron at the temperature of the Earth's inner core, Nature 413 (2001) 57–60.
[26] C.M.S. Gannarelli, D. Alfé, M.J. Gillian, The particle-in-cell model for ab initio thermodynamics: implication for the Earth's inner core, Phys. Earth Planet. Inter. 139 (2003) 243–253.
[27] A.K. Singh, H.K. Mao, J. Shu, R.J. Hemley, Estimation of single crystal elastic moduli from polycrystalline X-ray diffraction at high pressure: application to FeO and iron, Phys. Rev. Lett. 80 (1998) 2157–2160.
[28] H.R. Wenk, S. Matthies, R.J. Hemley, H.K. Mao, J. Shu, The plastic deformation of iron at pressures of the Earth's inner core, Nature 405 (2000) 1044–1047.
[29] F. Sette, G. Ruocco, M. Krisch, C. Masciovecchio, R. Verbeni, Collective dynamics in water by inelastic X-ray scattering, Phys. Scr., T 66 (1996) 48–56.
[30] N.W. Ashcroft, N.D. Mermin, Solid State Physics, Saunders College Publishing, USA, 1976.
[31] G. Fiquet, J. Badro, F. Guyot, H. Requardt, M. Krisch, Sound velocities in iron to 110 gigapascals, Science 291 (2001) 468–471.
[32] F. Birch, Composition of the Earth's mantle, Geophys. J. R. Astron. Soc. 4 (1961) 295–311.
[33] A.M. Dziewonsky, D.L. Anderson, Preliminary reference Earth model, Phys. Earth Planet. Inter. 25 (1981) 297–356.
[34] J.C. Crowhurst, A.F. Goncharov, J.M. Zaug, Impulsive stimulated light scattering from opaque materials at high pressure, J. Phys., Condens. Matter 16 (2004) S1137–S1142.
[35] H.K. Mao, J. Xu, V.V. Struzhkin, J. Shu, R.J. Hamley, W. Hu, M.Y. Hu, E.E. Alp, L. Vocadlo, D. Alfè, G.D. Price, M.J. Gillian, M. Schwoerer-Böhning, D. Häusermann, P. Eng, G. Shen, H. Giefers, R. Lübbers, G. Wortmann, Phonon density of states of iron up to 153 gigapascals, Science 292 (2001) 914–916.
[36] L.S. Dubrovinsky, N.A. Dubrovinskaia, S.K. Saxena, S. Rekhi, T. LeBihan, Aggregate shear moduli of iron up to 90 GPa and 1100 K, J. Alloys Compd. 297 (2000) 156–161.
[37] J.M. Brown, R.G. McQueen, Phase transitions, Gruneisen parameter and elasticity for shocked iron between 77 GPa and 400 GPa, J. Geophys. Res. 91 (1986) 7485–7494.
[38] E. Schreiber, O.L. Anderson, N. Soga, Elastic Constants and their Measurement, McGraw-Hill, New York, 1973.
[39] S.C. Singh, M.A.J. Taylor, J.P. Montagner, On the presence of liquid in Earth's inner core, Science 287 (2000) 2471–2474.
[40] D.C. Wallace, Thermodynamics of Crystals, Wiley, New York, 1972.